Light-sheet microscopy in thick media using scanned Bessel beams and two-photon fluorescence excitation

Florian Fahrbach, Vasily Gurchenkov, Kévin Alessandri, Pierre Nassoy, Alexander Rohrbach

Light-sheet microscopy in thick media using scanned Bessel beams and two-photon fluorescence excitation

Florian O. Fahrbach,[1,2,*] **Vasily Gurchenkov,**[3] **Kevin Alessandri,**[3] **Pierre Nassoy,**[3,4] **and Alexander Rohrbach**[1,5,6]

[1] *Laboratory for Bio- and Nano-Photonics, Department of Microsystems Engineering, University of Freiburg, Freiburg, Germany*
[2] *Max Planck Institute of Molecular Cell Biology and Genetics, Dresden, Germany*
[3] *Institut Curie, Centre de Recherche, F-75248 Paris, France*
[4] *LP2N, Institut d'Optique, CNRS UMR 5298 & Université de Bordeaux 1, F-33405 Talence, France*
[5] *Centre for Biological Signalling Studies (bioss), University of Freiburg, Freiburg, Germany*
[6] *rohrbach@imtek.de*
[*] *fahrbach@mpi-cbg.de*

Abstract: In this study we show that it is possible to successfully combine the benefits of light-sheet microscopy, self-reconstructing Bessel beams and two-photon fluorescence excitation to improve imaging in large, scattering media such as cancer cell clusters. We achieved a nearly two-fold increase in axial image resolution and 5-10 fold increase in contrast relative to linear excitation with Bessel beams. The light-sheet penetration depth could be increased by a factor of 3-5 relative to linear excitation with Gaussian beams. These findings arise from both experiments and computer simulations. In addition, we provide a theoretical description of how these results are composed. We investigated the change of image quality along the propagation direction of the illumination beams both for clusters of spheres and tumor multicellular spheroids. The results reveal that light-sheets generated by pulsed near-infrared Bessel beams and two photon excitation provide the highest image resolution, contrast and light-sheet penetration at a minimum amount of artifacts.

OCIS codes: (180.6900) Three-Dimensional microscopy; (180.4315) Nonlinear microscopy; (110.0113) Imaging through turbid media.

References and links

1. J. Huisken and D. Y. R. Stainier, "Selective plane illumination microscopy techniques in developmental biology," Development **136**, 1963–1975 (2009).
2. F. O. Fahrbach, P. Simon, and A. Rohrbach, "Microscopy with self-reconstructing beams," Nat. Photonics **4**, 780–785 (2010).
3. F. O. Fahrbach and A. Rohrbach, "A line scanned light-sheet microscope with phase shaped self-reconstructing beams." Opt. Express. **18**, 2608–2610 (2010).
4. T. A. Planchon, L. Gao, D. E. Milkie, M. W. Davidson, J. A Galbraith, C. G. Galbraith, and E. Betzig, "Rapid three-dimensional isotropic imaging of living cells using Bessel beam plane illumination." Nat. Methods. **8**, 417–423 (2011).
5. O. E. Olarte, J. Licea-Rodriguez, J. A. Palero, E. J. Gualda, D. Artigas, J. Mayer, J. Swoger, J. Sharpe, I. Rocha-Mendoza, R. Rangel-Rojo, and P. Loza-Alvarez, "Image formation by linear and nonlinear digital scanned light-sheet fluorescence microscopy with Gaussian and Bessel beam profiles." Biomed. Opt. Express. **3**, 1492–1505 (2012).

#187031 - $15.00 USD Received 18 Mar 2013; revised 23 Apr 2013; accepted 23 Apr 2013; published 31 May 2013

6. F. O. Fahrbach and A. Rohrbach, "Propagation stability of self-reconstructing Bessel beams enables contrast-enhanced imaging in thick media." Nat. Commun. **3**, 632 (2012).
7. L. Silvestri, A. Bria, L. Sacconi, G. Iannello, and F. S. Pavone, "Confocal light sheet microscopy: micron-scale neuroanatomy of the entire mouse brain," Opt. Express. **20**, 20582–20598 (2012).
8. E. Baumgart and U. Kubitscheck, "Scanned light sheet microscopy with confocal slit detection," Opt. Express **20**, 21805–21814 (2012).
9. J. Mertz, *Introduction to Optical Microscopy* (Roberts & Company Publishers,2010).
10. F. Helmchen and W. Denk. "Deep tissue two-photon microscopy," Nat. Methods **2**, 932-940 (2005).
11. P. Theer, M. T. Hasan, and W. Denk, "Two-photon imaging to a depth of 1000m in living brains by use of a Ti:Al2O3 regenerative amplifier," Opt. Lett. **28**, 1022–1024 (2003).
12. E. Beaurepaire, M. Oheim, and J. Mertz, "Ultra-deep two-photon fluorescence excitation in turbid media," Opt. Commun. **188**, 25–29 (2001).
13. J. Palero, S. I. C. O. Santos, D. Artigas, and P. Loza-Alvarez. "A simple scanless two-photon fluorescence microscope using selective plane illumination," Opt. Express **18**, 8491–8498 (2010).
14. T. V. Truong, W. Supatto, D. S. Koos, J. M. Choi, and S. E. Fraser, "Deep and fast live imaging with two-photon scanned light-sheet microscopy," Nat. Methods **8**, 757–760 (2011).
15. E. Botcherby, R. Juskaitis, and T. Wilson, "Scanning two photon fluorescence microscopy with extended depth of field," Opt. Commun. **268**, 253–260 (2006).
16. P. Dufour, M. Pich, Y. De Koninck, and N. McCarthy, "Two-photon excitation fluorescence microscopy with a high depth of field using an axicon," Appl. Opt. **45**, 9246–9252 (2006).
17. A. Rohrbach, "Artifacts resulting from imaging in scattering media: a theoretical prediction," Opt. Lett. **34**, 3041–3043 (2009).
18. J. A. Fleck, J. R. Morris, and M. D. Feit, "Time-dependent propagation of high energy laser beams through the atmosphere." Appl. Phys. **10**, 129–160 (1976).
19. M. D. Feit and J. A. Fleck, "Light propagation in graded-index optical fibers," Appl. Opt. **17**, 3990–3998 (1978).
20. C. D. Bohren and D. R. Huffman, *Absorption and Scattering of Light by Small Particles* (Wiley-VCH, Berlin, 1998).

1. Introduction

The generation of high-quality three-dimensional images in large scattering media such as tissue, embryos, plants, or cell clusters in biology is a tricky task. Limited penetration and scattering of illumination light inside the specimen degrade the image quality. Moreover, unnecessary photo-bleaching of fluorophores that are not in the image plane degrade the usability of microscopes. In this context, light-sheet based microscopy [1] offers the decisive advantage that only those parts of the object are illuminated that are in the plane of focus of an objective lens (OL). Sample illumination by a thin sheet of light reduces fluorophore bleaching significantly relative to conventional epi-fluorescence microscopy or point-scanning confocal microscopy. Recently it has been shown that an alternative form of light-sheets can be generated by using laterally scanned Bessel beams [2–5], which revealed an increased penetration depth of illumination light in thick media of up to 50% [2, 3]. However the advantage of beam self-reconstruction in scattering media is at the cost of a decreased image contrast: the Bessel beam's ring system, which contains the photons necessary for beam-healing, excites fluorescence above and below the plane of focus. Exploiting the propagation stability of Bessel beams allowed to increase image contrast very efficiently. The confocal-line detection principle, where out-of-focus fluorescence excited by the ring system is largely blocked [6] also rejects scattered light. Therefore, this principle is also useful in combination with Gaussian beam illumination [7, 8].

However, an alternative approach would be desirable, where a thin light-sheet does not generate any out-of-focus fluorescence. Two-photon excitation (TPE) of the fluorophores is such a method that avoids the contrast degrading effect of the ring system. In TPE, two near-infrared (NIR) photons must hit the same fluorophore at the same time to excite it [9]. The resulting quadratic dependence of the fluorophore emission $F(\mathbf{r})$ on the illumination intensity $h_{\mathrm{ill}}(\mathbf{r})$ is expected to suppress the fluorescence in the ring system efficiently. In addition, the nearly doubled wavelength of the NIR excitation light should reduce scattering and increase the penetration depth similarly to point scanning TPE fluorescence microscopy [10–12].

#187031 - $15.00 USD Received 18 Mar 2013; revised 23 Apr 2013; accepted 23 Apr 2013; published 31 May 2013

The favorable combination of light-sheet microscopy and TPE has been employed by other groups using static light-sheets [13], scanned Gaussian beams [14] and Bessel beams [4, 5]. Moreover, TPE by Bessel beams in point-scanning systems were used, but only to increase the depth of focus of the system [15, 16]. The results presented here are the first investigation of TPE by Bessel beams in thick and strongly scattering media using a light-sheet microscope. This combination is especially interesting since on the one hand the light-sheet microscope is an ideal tool to study the propagation of beams in scattering media because the propagation of illumination light within the detection focal plane can be observed from the side. On the other hand, only at depths of several hundred microns inside scattering media the following three advantages can take effect efficiently: the reduced photo-bleaching enabled by light-sheet microscopy, weaker scattering artifacts due to the self-reconstruction capability of the Bessel beams and increased contrast due to the TPE principle.

We demonstrate the performance of this approach in tumor cell clusters. The motivation for observing this form of cancerous tissue in a light-sheet microscope is the following: The discovery of new anticancer drugs requires High Throughput Screening (HTS) approaches. These are usually based on animal models, which generally well recapitulate the main features of human tumors. 2D-cell based in-vitro models have been extensively used in preclinical drug screening despite their poor predictive capability for in-vivo efficacy. 3D-tissue culture models, on the other side, are undisputedly better candidates to reconcile scientific, medical and ethical requirements. Multicellular Tumor Spheroids (MCTS), which were shown to be superior in-vitro tumor models as compared to 2D cell monolayers, have not yet received widespread application in cancer biology. Beside the technical difficulty of massively producing size-controlled spheroids, another limitation for their more extensive use originates from the difficulty to image thick and highly scattering samples with reduced photo-toxicity over several days. To decipher the molecular and cellular mechanisms of (in-vitro) tumor progression, imaging techniques are required that allow investigating not only the rim of peripheral cells, but also the core of the spheroid, to fully observe the spatial and temporal organization of the whole tumor mimics.

In this paper we describe briefly the technical setup of a microscope able to fully image tumor multicellular spheroids. We explain and illustrate all necessary principles and give a detailed mathematical description of the simulated and measured results or phenomena. We compare the non-diffraction capability of single (1p) and two (2p) - photon fluorescence excitation Bessel beams in homogeneous media as well as their self-reconstruction properties in scattering media. We analyze contrast and resolution for both beam types. In the last section of this paper, we demonstrate the strong benefits of 2p-Bessel beams both in widefield and confocal-line detection mode - for light-sheet microscopy in 250μm large biological tumor cell clusters.

2. Experimental setup

In order to be able to compare the performance of various beams for linear and non-linear fluorescence excitation in a light-sheet microscope we expanded our existing setup (which is described in detail in [3]) by a Ti-Sapphire-Laser (Chameleon, Coherent). This laser emits short pulses with a duration of 140fs with a repetition rate of 80MHz with high power ($P_{\mathrm{avg}} >$ 1W) over a wide range in the near-infrared spectral range (720nm to 920nm). The setup for TPE fluorescence is sketched in Fig. 1. A switchable mirror allows quick alteration between illumination by the visible lasers and the NIR laser. All optical elements (mirror, lenses) are suitable for the usage in the NIR range and for the high peak intensities generated by the pulsed laser. Even though the achromatic doublets (Qioptiq) are optimized for the visible spectral range, neither reflections due to the imperfect anti-reflection coating nor aberrations to the illumination beams were observed. A broadband LCOS-based spatial light modulator (SLM) was chosen (Pluto NIR II, Holoeye) which is optimized for a wide spectral range (400-1100nm)

#187031 - $15.00 USD Received 18 Mar 2013; revised 23 Apr 2013; accepted 23 Apr 2013; published 31 May 2013

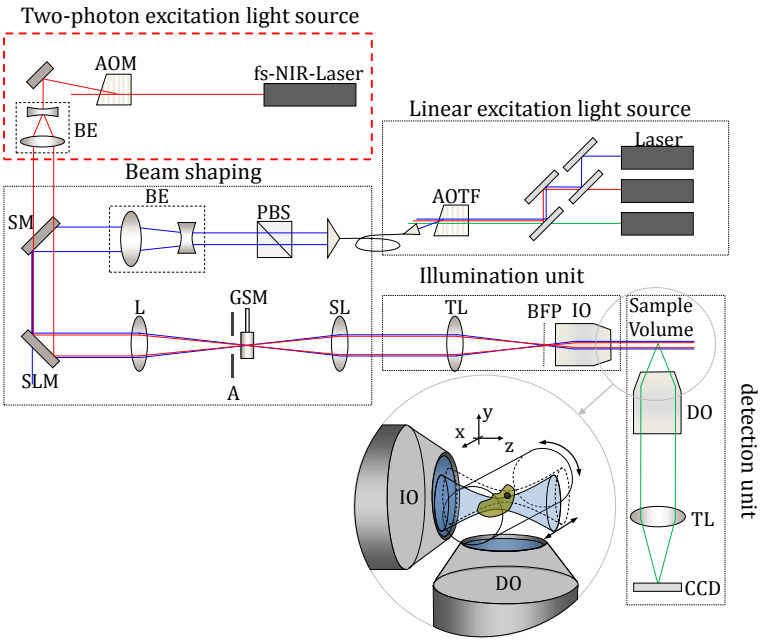

Fig. 1. **Sketch of the experimental setup.** The setup is equipped with laser units for both linear and two-photon fluorescence excitation. Acousto-optic modulators (AOM) or tunable filters (AOTF) are used to steer the beam power. After passing beam expanders (BE), polarizing beam splitters (PBS) and mirrors (M), a spatial light modulator (SLM) holographically shapes the phase of the incoming Gaussian laser beams. An aperture (A) removes unwanted diffraction orders. The galvanometric scanning mirror (GSM) deflects the beam in a plane conjugate to back-focal-plane (BFP) of the illumination objective (IO) via the scanning lens (SL) and tube lens (TL). In the detection unit fluorescence light emitted in the sample volume is imaged via the detection objective (DO) and another TL onto the CCD camera.

and thereby enabled us to compare phase shaped beams in the visible and NIR range. For all measurements, a 40x/0.8 lens (W Achroplan, Zeiss) was used.

3. Light-sheets by scanned illumination beams and resulting fluorescence

In the following, we investigate both theoretically and experimentally the fluorescence excitation of differently labeled objects. The fluorophore distribution $c_{\mathrm{F}}(\mathbf{r})$ at position $\mathbf{r}$ inside the illuminated part of the object can be either constant, $c_{\mathrm{F}}(\mathbf{r}) = c_0$, as in the case of a homogeneous fluorescein solution. Alternatively, $c_{\mathrm{F}}(\mathbf{r})$ can vary abruptly as in the case of fluorescent spheres in a non-fluorescent medium or non-fluorescent spheres embedded in a fluorescent gel. And third, $c_{\mathrm{F}}(\mathbf{r})$ can vary relatively smoothly as in the case of stained dense cell clusters. The resulting fluorescence intensity distribution $F(\mathbf{r})$ is modulated by $c_{\mathrm{F}}(\mathbf{r})$, by the excitation cross section $\sigma_{1\mathrm{p}}$ for linear and σ_{2p} for two photon excitation, as well as by the excitation intensity $h_{\mathrm{ill}}(\mathbf{r})$. We find both for the linear and for the non-linear fluorescence:

$$F_{1\mathrm{p}}(\mathbf{r}) = c_{\mathrm{F}}(\mathbf{r}) \cdot \sigma_{1\mathrm{p}} \cdot h_{\mathrm{ill},1}(\mathbf{r}) \quad (1)$$

$$F_{2\mathrm{p}}(\mathbf{r}) = c_{\mathrm{F}}(\mathbf{r}) \cdot \sigma_{2\mathrm{p}} \cdot h_{\mathrm{ill},2}(\mathbf{r})^2. \quad (2)$$

Since two photons have two arrive independently of each other during the life-time of the fluorophore's virtual excitation state, the photons' probabilities to hit the fluorophore's cross

#187031 - $15.00 USD Received 18 Mar 2013; revised 23 Apr 2013; accepted 23 Apr 2013; published 31 May 2013

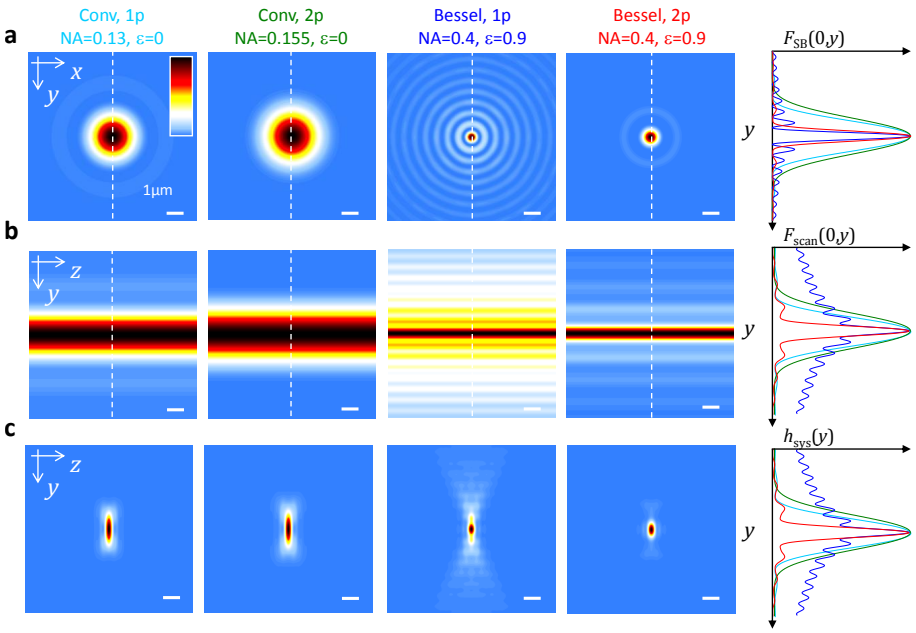

Fig. 2. **Simulated fluorescent beam profiles.** Simulated fluorescence cross-sections $F(x,y)$ for different types of illumination beams with the same depth of field along the illumination z-axis. A Gaussian beam for one-photon (1st column) and two-photon excitation (2nd column) and a Bessel beam for one-photon (3rd column) and two-photon excitation (4th column). a) Single beam fluorescence intensity $F(x,y,0)$ and the corresponding line scans $F(0,y,0)$ on the right. b) Light sheet fluorescence produced by a lateral scan $\int F(x,y,0)\,dx$ of the three beams in x-direction and line profiles $\int F(0,y,0)\,dx|_{x=0}$ through the light-sheets. c) Multiplications of the light-sheets with the detection point-spread function $h_{\mathrm{det}}(x,z)$.

section must be multiplied with each other. This results in the quadratic dependence of the illumination intensity, $h_{\mathrm{ill},2}(\mathbf{r})^2$, as described in Eq. (2). For the typical case of pulsed illumination light, a more precise description of the temporally averaged fluorescence would be $\langle F_{1\mathrm{p}}(\mathbf{r})\rangle = c_{\mathrm{F}}(\mathbf{r})\cdot\sigma_{2\mathrm{p}}\cdot G\cdot\langle h_{\mathrm{ill},2}(\mathbf{r})^2\rangle$, where G is a correction factor [9]. However, keeping this in mind and disregarding dispersive effects, we hold on to the expression of Eq. (2).

In many cases, the resulting fluorescence $F(\mathbf{r})$ in a homogeneously stained sample illustrates well the excitation intensity $h_{\mathrm{ill}}(\mathbf{r})$, if the detection PSF is small enough. Figure 2 displays simulation results of linear and nonlinear fluorescence excitation by Gaussian beams and Bessel beams at λ_1 and λ_2, respectively. The depth of field of the fluorescence excitation $\Delta z = 100\mu$m is equal for all beams. As described in the Appendix, due to the different wavelengths used, the illumination beams, $h_{\mathrm{ill},1}(\mathbf{r})$, and $h_{\mathrm{ill},2}(\mathbf{r})$, have to be designed differently to match their depth-of-field. The cross sections, $F(x,y,z=0)$ and the intensity line scans $F(0,y,0)$ reveal the relatively large widths of the Gaussian beam (green line), the narrow main lobe of the Bessel beam with distinct side lobes from the ring system (blue line) and the narrow profile of the two photon (2p) Bessel beam (red line), where the rings are strongly suppressed.

By continuously displacing the illumination beam $h_{\mathrm{ill}}(\mathbf{r})$ by b_x in lateral x-direction the re-

#187031 - $15.00 USD Received 18 Mar 2013; revised 23 Apr 2013; accepted 23 Apr 2013; published 31 May 2013

sulting 1p- and 2p- fluorescence distributions are

$$F_{1p}(\mathbf{r}) = c_F(\mathbf{r}) \cdot \sigma_{1p} \cdot \int_{x_m}^{x_m} h_{ill,1}(x-b_x, y, z)\, db_x \quad (3)$$

$$F_{2p}(\mathbf{r}) = c_F(\mathbf{r}) \cdot \sigma_{2p} \cdot \int_{x_m}^{x_m} h_{ill,2}(x-b_x, y, z)^2\, db_x. \quad (4)$$

These dependencies are displayed in Fig. 2(b) for the four types of beams and a homogeneous fluorophore concentration $c_F(\mathbf{r}) = c_0$. The profiles $F_{scan}(0,y,0)$ through the light-sheet in the right part of Fig. 2(b) reveal the increased width of the light-sheet relative to the width of a single beam for the 1p-Bessel beam. This effect is hardly visible for the 2p-Bessel light-sheet.

In the last step of the image generation process, fluorescence is detected by the detection objective (DO) with NA_{det} and point-spread function h_{det} and imaged onto the camera. Mathematically, the 3D image $p(b_y, r)$ for a light-sheet shifted vertically by b_y is obtained by $F_{1p}(b_y, \mathbf{r}) * h_{det}(\mathbf{r})$, where $*$ denotes the convolution, which corresponds to a low-pass filtering of the fluorophore distribution $F(b_y, \mathbf{r})$ especially along the detection y-axis. The images read

$$p_{1p}(b_y, \mathbf{r}) = \left(c_F(\mathbf{r}) \cdot \sigma_{1p} \cdot \int_{x_m}^{x_m} h_{ill,1}(x-b_x, y-b_y, z) db_x \right) * h_{det}(\mathbf{r}) \quad (5)$$

$$p_{2p}(b_y, \mathbf{r}) = \left(c_F(\mathbf{r}) \cdot \sigma_{2p} \cdot \int_{x_m}^{x_m} h_{ill,2}(x-b_x, y-b_y, z)^2 db_x \right) * h_{det}(\mathbf{r}). \quad (6)$$

The image of a point-like fluorophore, $c_F(\mathbf{r}) = c_0\, \delta(\mathbf{r})$ illuminated by a light-sheet at position $b_y = 0$ is shown in Fig. 2(c) and demonstrates the suppression of out-of-focus fluorescence for the 2p-Bessel beam, but not for the 1p-Bessel beam.

The numerical results are confirmed experimentally by the 2D-images of single beams $p_{1p}(x,0,z) = c_0 \cdot \sigma_{1p} \cdot h_{ill,1}(\mathbf{r}) * h_{det}(\mathbf{r})\big|_{y=0}$ and $p_{2p}(x,0,z) = c_0 \cdot \sigma_{2p} \cdot h^2_{ill,2}(\mathbf{r}) * h_{det}(\mathbf{r})\Big|_{y=0}$, focused at $NA_{ill} \approx 0.3$, that excite fluorescence in a homogeneous fluorescein solution. As demonstrated by the experimental data shown in Fig. 3, single-photon fluorescence excitation generates strong fluorescence in the Bessel beam's ring system shown in Fig. 3(a), which is still well visible due to the narrow $h_{det}(\mathbf{r})$ at a Numerical Aperture $NA_{det} = 0.8$ of the detection lens. In the two-photon case, fluorescence from the ring system is strongly suppressed as can be seen in Fig. 3(b), which is also shown by the lateral profiles through the beam images shown in Fig. 3(c).

4. Light scattering during propagation through inhomogeneous media

In most applications of light-sheet microscopy the refractive index variations inside the object are not index-matched (cleared). Illumination and detection light are scattered at each refractive index change, which leads to a new propagation direction of each scattered photon. Only a small fraction of the photons remain unscattered, so-called ballistic photons, while the other photons are scattered very many times such that these photons become diffusive. The corresponding electromagnetic field of the illumination beam is split into an incident and a scattered electric field, $E_i(\mathbf{r})$ and $E_s(\mathbf{r})$, such that the fluorescence intensity $F_{1p}(\mathbf{r}) \propto h_{ill,1}(\mathbf{r})$ can be expressed as:

$$\begin{aligned} F_{1p}(\mathbf{r}) &= c_F(\mathbf{r}) \cdot \sigma_{1p} \cdot h_{ill,1}(\mathbf{r}) \\ &= c_F(\mathbf{r}) \cdot \sigma_{1p} \cdot \left| E_{i,1}(\mathbf{r}) + E_{s,1}(\mathbf{r}) \right|^2 \\ &= c_F(\mathbf{r}) \cdot \sigma_{1p} \cdot \left[|E_{i,1}|^2 + \left(|E_{s,1}|^2 + 2\cos\left(|E_{i,1}||E_{s,1}| \right) \left(\phi_{i,1}(\mathbf{r}) - \phi_{s,1}(\mathbf{r}) \right) \right) \right] \\ &= c_F(\mathbf{r}) \cdot \sigma_{1p} \cdot \left(h_{i,1}(\mathbf{r}) + h_{s,1}(\mathbf{r}) \right). \end{aligned} \quad (7)$$

#187031 - $15.00 USD Received 18 Mar 2013; revised 23 Apr 2013; accepted 23 Apr 2013; published 31 May 2013

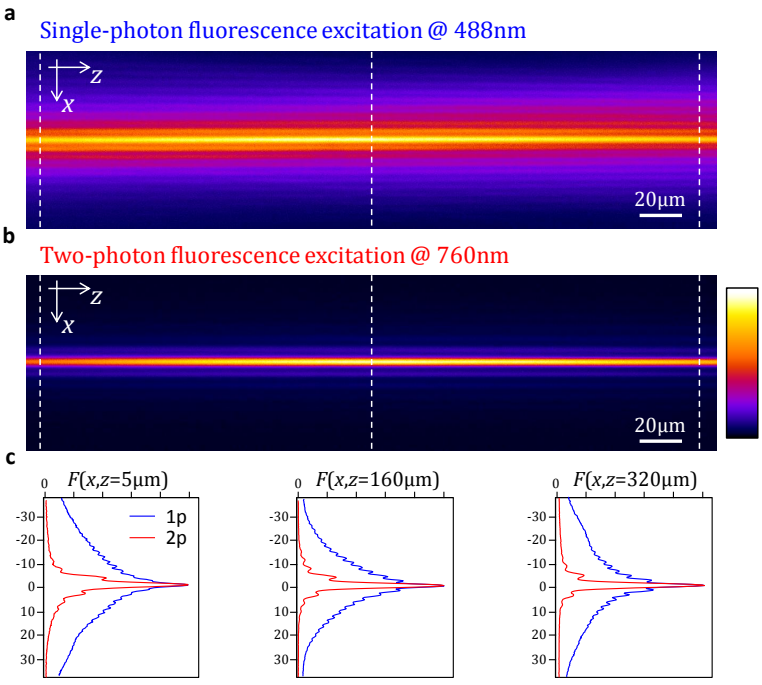

Fig. 3. **Measured linear and non-linear fluorescence excitation.** The fluorescence excited by Bessel beams over a distance in a fluorescein solution is shown for linear fluorescence excitation (a) and TPE (b). In the linear case, the Bessel beams ring system is strongly visible. In contrast, in the case of TPE the ring system is efficiently suppressed so that fluorescence is excited almost exclusively by the beams main lobe. This effect is quantified by the line-scans shown in (c), where hardly any changes in the profiles for different distances z are visible.

Corresponding to Eq. (1), these equations show that the illumination intensity $h_{\mathrm{ill}}(\mathbf{r})$ can be split into two terms: $h_{\mathrm{i}}(\mathbf{r})$ and $h_{\mathrm{s}}(\mathbf{r})$ both illuminate the object [17]. Thereby two images are generated by convolution of the object $c_{\mathrm{F}}(\mathbf{r})$ with the detection PSF:

$$p(\mathbf{r}) = ((h_i(\mathbf{r}) + h_s(\mathbf{r})) \cdot c_{\mathrm{F}}(\mathbf{r}) \cdot \sigma) * h_{\mathrm{det}}(\mathbf{r}) = p_{\mathrm{ideal}}(\mathbf{r}) + p_{\mathrm{ghost}}(\mathbf{r}) \tag{8}$$

The second image is called the ghost image and needs to be minimized by clever illumination or detection techniques. In the two-photon case the sum of the ideal and the scattered illumination beams can be expressed as

$$\begin{aligned} F_{2\mathrm{p}}(\mathbf{r}) &= c_{\mathrm{F}}(\mathbf{r}) \cdot \sigma_{2\mathrm{p}} \cdot h_{\mathrm{ill},2}(\mathbf{r})^2 \\ &= c_{\mathrm{F}}(\mathbf{r}) \cdot \sigma_{2\mathrm{p}} \cdot (h_{\mathrm{i},2}(\mathbf{r}) + h_{\mathrm{s},2}(\mathbf{r}))^2 \\ &= c_{\mathrm{F}}(\mathbf{r}) \cdot \sigma_{2\mathrm{p}} \cdot h_{\mathrm{i},2}(\mathbf{r})^2 + c_{\mathrm{F}}(\mathbf{r}) \cdot \sigma_{2\mathrm{p}} \cdot \left(h_{\mathrm{s},2}(\mathbf{r})^2 + 2 \cdot h_{\mathrm{i},2}(\mathbf{r}) \cdot h_{\mathrm{s},2(\mathbf{r})}\right). \end{aligned} \tag{9}$$

The first term in Eq. (9) corresponds to Eq. (2), whereas the second term represents unwanted two-photon fluorescence excitation in the object. In the two-photon case the ghost image can be expressed mathematically as

$$p_{\mathrm{ghost}}(\mathbf{r}) = \left(c_{\mathrm{F}}(\mathbf{r}) \cdot \sigma_{2\mathrm{p}} \cdot \left(h_{\mathrm{s},2}(\mathbf{r})^2 + 2 \cdot h_{\mathrm{i},2}(\mathbf{r}) \cdot h_{\mathrm{s},2}(\mathbf{r})\right)\right) * h_{\mathrm{det}}(\mathbf{r}) \rightarrow \min. \tag{10}$$

Theoretically, p_{ghost} approaches a minimum when the illumination beam intensity becomes minimal or when the following two terms approach each other $h_{\mathrm{s},2}^2(\mathbf{r}) \rightarrow 2 \cdot h_{\mathrm{i},2}(\mathbf{r}) \cdot h_{\mathrm{s},2}(\mathbf{r})$.

#187031 - $15.00 USD Received 18 Mar 2013; revised 23 Apr 2013; accepted 23 Apr 2013; published 31 May 2013

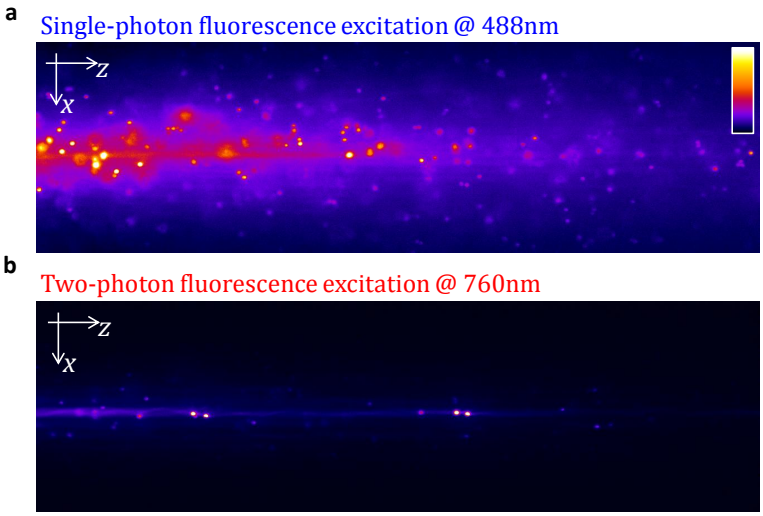

Fig. 4. **Measured fluorescence excited by a Bessel beam in a scattering medium.** The fluorescence excited by Bessel beams over a distance of 320μm in a slightly fluorescent gel containing fluorescent 0.75μm polystyrene spheres is shown for linear fluorescence excitation (a) and for TPE (b). In the linear case, the Bessel beams ring system illuminates many spheres outside the Bessel beams main lobe. For TPE, fluorescence excitation by the ring system and by scattered light is suppressed so that mainly spheres along a thin line corresponding to the Bessel beams main lobe are visible.

The fluorophore distributions described by Eq. (7) and Eq. (9) were measured by using a cluster of fluorescent 0.75μm polystyrene spheres embedded in a slightly fluorescent gel as shown in Fig. 4. Whereas in the single-photon case the Bessel beam excites a lot of unwanted fluorescence, i.e. fluorescence outside the main lobe of the Bessel beam, this unwanted fluorescence is hardly visible in the two-photon case.

By inspecting the two beams propagating through the inhomogeneous medium shown in Fig. 4, the effect of a decaying intensity manifests. This results from a decreasing number of ballistic photons along the beam axis, i.e. the propagation direction z. As shown recently [2] the axial fluorescence intensity $F_{1p}(z)$ falls off approximately exponentially also for Bessel beams propagating through scattering media:

$$\begin{aligned} F_{1p}(z) &\approx c_0 \cdot \sigma_{1p} \cdot h_{ill,1}(z=0) \cdot \exp\left\{-(\mu_{abs,1}+\mu_{sca,1}) \cdot z\right\} \\ &= c_0 \cdot \sigma_{1p} \cdot (h_{i,1}(z)+h_{s,1}(z)) \end{aligned} \tag{11}$$

Here we assumed an approximately homogeneous fluorophore concentration $c_F(z) \approx c_0$ and integrated $F_{1p}(z) = \int F_{1p}(x,y,z)\,dxdy$ over a sufficiently broad area. $\mu_{sca,1} = \mu_{sca}(\lambda_1) = \mu'_{sca,1} \cdot (1-g)$ is the effective scattering coefficient and $\mu_{abs,1} = \mu_{abs}(\lambda_1)$ the coefficient for the light absorption mainly by fluorophores. The anisotropy factor $g = g(a \cdot n_s/\lambda)$ reduces the intensity loss along z due to scattering (a is the radius, n_s is the refractive index of the scatterer). For larger scatterers with $a \cdot n_s > \lambda$ we find for where ($\lambda_1 = 488$nm, $\lambda_2 = 800$nm) the anisotropy factors $g \to 1$ as e.g. $g(0.75\mu\text{m} \cdot 1.59/\lambda_1) = 0.92$, $g(0.75\mu\text{m} \cdot 1.59/\lambda_2) = 0.85$, $g(2\mu\text{m} \cdot 1.41/\lambda_1) = 0.99$ or $g(2\mu\text{m} \cdot 1.41/\lambda_2) = 0.97$

In the two-photon case the axial decrease in illumination intensity can be described as $\frac{1}{c_0 \cdot \sigma_{2p}} \cdot \frac{d}{dz} F_{2p}(z) \approx -\mu_{abs,2} \cdot h_{ill,2}(z)^2 - \mu_{sca,2} \cdot h_{ill,2}(z)$ owing to the light absorbance by fluorophores according to $\mu_{abs,2} \cdot h_{ill,2}^2$ and to a loss in scattering according to $\mu_{sca,2} \cdot h_{ill,2}$. Solving the latter

#187031 - $15.00 USD Received 18 Mar 2013; revised 23 Apr 2013; accepted 23 Apr 2013; published 31 May 2013

differential equation leads to an expression with an axial intensity decay, which is similar to an exponential, but reads

$$h_{\mathrm{ill},2}(z) \approx \frac{h_{\mathrm{ill},2}(0)}{e^{\mu_{\mathrm{abs},2}\cdot z} + h_{\mathrm{ill},2}(0)\cdot \mu_{\mathrm{abs},2}/\mu_{\mathrm{sca},2}\cdot (e^{\mu_{\mathrm{abs},2}\cdot z}-1)} \tag{12}$$

Assuming an average fluorophore density independent of z (as in Fig. 4), we hardly noticed any axial decay and estimate the intensity loss due to absorption by fluorophores to be small such that $\mu_{\mathrm{abs},2}\cdot h_{\mathrm{ill},2}(z) \ll \mu_{\mathrm{sca},2}$. Therefore we can approximate the fluorescence decay in axial direction for the two-photon case to be

$$F_{2\mathrm{p}}(z) \approx c_0 \cdot \sigma_{2\mathrm{p}} \cdot h_{\mathrm{ill},2}(z)^2 \approx c_0 \cdot \sigma_{2\mathrm{p}} \cdot h_{\mathrm{ill},2}(0)^2 \cdot \exp(-2\mu_{\mathrm{sca},2}\cdot z) \tag{13}$$

For Rayleigh scatterers, the scattering coefficient varies as $\mu_{\mathrm{sca}}(\lambda) \propto \lambda^{-4}$, whereas for larger scatterers in the size range of the incident wavelength one finds $\mu_{\mathrm{sca}}(\lambda) \propto \lambda^{-2}$ (this can be easily proven with Mie-theory [20]). Therefore we approximate $\mu_{\mathrm{sca}}(\lambda_2) \approx (\lambda_1/\lambda_2)^2 \cdot \mu_{\mathrm{sca}}(\lambda_1)$. For $\lambda_1 = 488$nm and $\lambda_2 = 800$nm we obtain $\mu_{\mathrm{sca}}(\lambda_2) \approx 0.37\mu_{\mathrm{sca}}(\lambda_1)$. Based on this rough estimate, a Bessel beam with $\lambda_2 = 800$nm wavelength has an only $1/(2\times 0.37) = 1.34$ fold increased penetration depth $d_2 = 1/(2\mu_{\mathrm{sca},2})$ relative to a Bessel beam at $\lambda_1 = 488$nm where $d_1 = 1/\mu_{\mathrm{sca},1}$. For $\lambda_2 = 920$nm, one can expect $d_2 > 1.8d_1$. We will show in the following that this ratio of penetration depths can be confirmed experimentally by imaging fluorescent beads and labelled cancer cell clusters.

5. Artifacts in non-linear light-sheet microscopy

A quadratic fluorescence dependence on the excitation intensity has two effects. On the one hand it suppresses the unwanted fluorescence in a controlled manner, for example from the Bessel beam ring system. On the other hand, it might increase image artifacts such as the frequently occurring stripes resulting from the interference of scattered and unscattered light. To investigate the strength of the two effects, we used the beam propagation method (BPM) [18,19] to simulate the propagation of various illumination beams through a cluster of non-fluorescent glass spheres with a diameter $d = 2\mu$m that are embedded in a fluorescing environment. From the expressions in Eq. (7) and Eq. (9) describing the fluorescence distribution for linear and non-linear excitation, respectively, we derived the ghost image in Eqs. (8) and (10).

The results for horizontal and vertical cross-sections, $p(x,y_0,z)$ and $p(x_0,y,z)$, through the 3D image stacks are displayed in Fig. 5(a)-(d). By simulating the ideal image, shown in Fig. 5(e) that results from illumination by a homogenous, non-scattered light-sheet with a thickness of only 0.2μm, we can easily generate the unwanted ghost image by subtraction of the real image (compare Eq. (8)). The lateral standard deviations of the ideal and the ghost image as a function of the propagation distance z are shown in Fig. 5(f) and (g), respectively (see also [2]). From these values we can estimate the image quality by calculation of the parameter Q_{art}, which we define as follows:

$$Q_{\mathrm{art}} = \frac{\Delta p_{\mathrm{ideal}}}{\Delta p_{\mathrm{ghost}}} = \frac{\sqrt{\frac{1}{N-1}\sum_{x,z}\left(p_{\mathrm{ideal}}(x,z) - p_{\mathrm{ideal}}\right)}}{\sqrt{\frac{1}{N-1}\sum_{x,z}\left(p_{\mathrm{ghost}}(x,z) - p_{\mathrm{ghost}}\right)}} \tag{14}$$

A good light-sheet generates high contrast in the ideal image ($\hat{s}_{\mathrm{ideal}}$ is large) and a low contrast in the ghost image ($\hat{s}_{\mathrm{ghost}}$ is small). By inspecting Fig. 5, one can recognize two things: illumination in the case of the 2p-Bessel beam results in the highest value $Q_{\mathrm{art}} = 0.66$ and secondly, most sphere images, especially those indicated by white arrows (i and ii), are reproduced at best by the 2p-Bessel beam image.

#187031 - $15.00 USD Received 18 Mar 2013; revised 23 Apr 2013; accepted 23 Apr 2013; published 31 May 2013

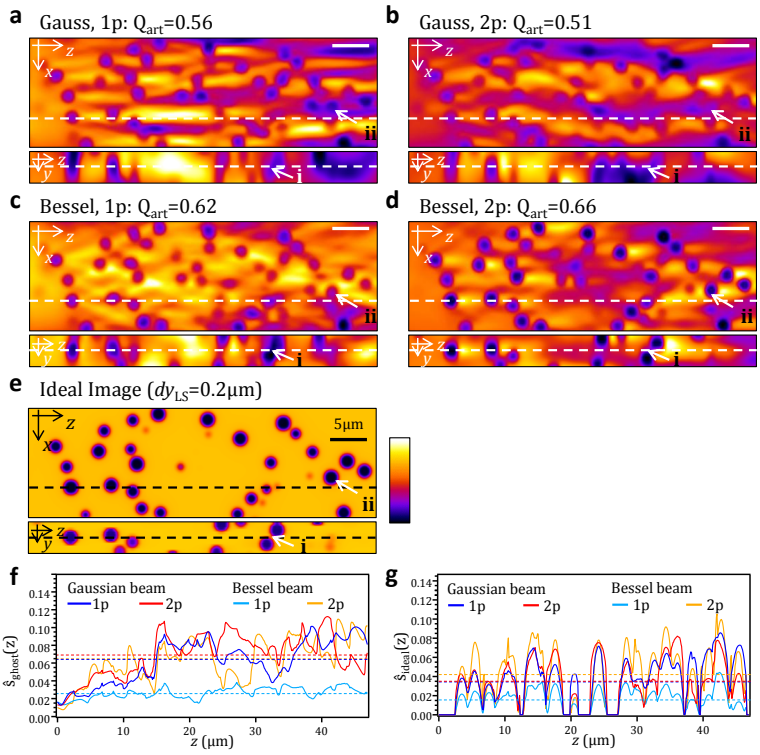

Fig. 5. **Simulated images of beads embedded in a fluorescing gel illuminated with four different beams.** All beams propagate in z-direction (from left to the right). Each image $p(x, y_0, z)$ is shown above a cross-section $p(x_0, y, z)$ along the detection axis. The positions x_0 and y_0 are indicated by dashed lines. a) 1p- Gaussian beam. b) 2p- Gaussian beam. c) 1p- Bessel beam. d) 2p- Bessel beam. e) 200nm thin ideal light sheet without scattering. The LUT of the images is auto-scaled so that they express the relation between the amplitude of the artifacts and the images of the spheres. Note that no information on the absolute image contrast can be drawn from these images. f, g) the lateral standard-deviation of the ideal and the ghost image for all four imaging modes, according to Eq. (14) derived in [2]. Q_{art} gives the ratio of the total lateral standard-deviations of the ideal and the ghost images according to Eq. (14).

6. Resolution and contrast in a scattering sample

To assess resolution and image contrast inside of a scattering medium we image a volume containing fluorescing polystyrene spheres (diameter 0.75μm). The spheres were embedded in nonfluorescent gel and imaged for linear and nonlinear fluorescence excitation by Bessel beams at $NA_{\mathrm{ill}} \approx 0.3$. An image projection $\sum_y p(x,z)$ along the detection y-axis is shown in Figs. 6(a,d) together with a projection $\sum_x p(y,z)$ along the beam-scanning x-axis in Figs. 6(b,e). It can be clearly seen that sectioning and axial resolution is greatly enhanced over a distance of more than 300μm by nonlinear fluorescence excitation over linear excitation by a Bessel beam. The images of the spheres are significantly smaller along the detection axis without any remarkable degradation along the propagation direction (Figs 6(b,e)). The two image magnifications shown in Figs 6c, f reveal the shape and the extent of the sphere images, which come close to the expected shapes of the detection point- spread-function $h_{\mathrm{det}}(\mathbf{r})$. This confirms that beam self-reconstruction works well in large scattering media both for single-photon and two-photon

#187031 - $15.00 USD Received 18 Mar 2013; revised 23 Apr 2013; accepted 23 Apr 2013; published 31 May 2013

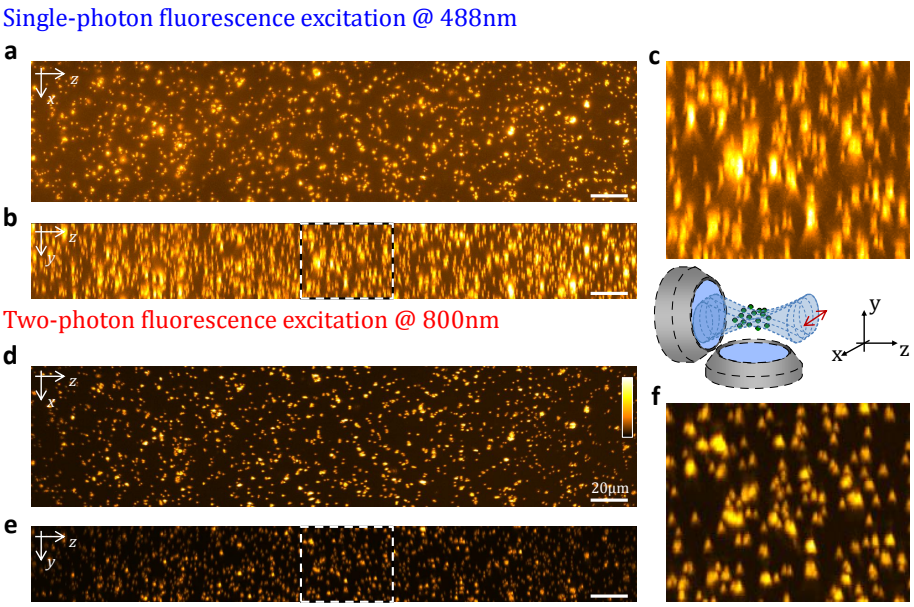

Fig. 6. **Measured images of fluorescing spheres for linear and two-photon Bessel beam excitation.** Measured images of fluorescing polystyrene spheres ($d = 0.75\mu$m) embedded in a gel illuminated with two different Bessel beams, which propagate from left to right. The image projection $\sum_y p(x,z)$ along the detection axis y is shown above the projection $\sum_x p(y,z)$ along x. a) single photon fluorescence excitation and b) two-photon fluorescence excitation. Magnification for single-photon excitation and two-photon excitation taken from the area marked by a dashed rectangle in b) and e) are shown in c) and f), respectively. The total size of the image to volume is 75μm$x40\mu$m$x325\mu$m.

excitation.

The signal-to-background ratio $p_S/p_{BG}(z)$ as well as the axial resolution $dy_{1/e}(z)$ are analyzed in more detail using profiles through images of ≈ 1200 spheres. We fitted a Gaussian function to each profile $p(y)$ extracted at the (x,z)-position of a sphere as in [6]. Figure 7(a) shows that the signal-to-background ratio $p_S/p_{BG}(z)$ is significantly higher than in the case of two-photon excitation revealing only a small drop-off for high propagation distances $z > 250\mu$m. By analyzing the axial $1/e$-widths of the bead images, $dy_{1/e}$, we find an average width of $\langle dy_{1/e} \rangle \approx 2\mu$m for the single photon illumination, whereas for TPE the average widths $\langle dy_{1/e} \rangle \approx 1\mu$m are by a factor of two smaller. Note that over a propagation distance of more than 300μm hardly any drop-off in resolution is visible.

7. Light-sheet imaging of tumor multicellular spheroids using two-photon fluorescence excitation

The so far discussed image quality parameters such as resolution, contrast, scattering artifacts, or light-sheet penetration depth have been investigated theoretically or by computer simulations and have been confirmed by experiments using bead clusters. However, although their ideal images remain unknown, high-quality imaging of large, scattering biological specimen is the primary goal in fluorescence microscopy. Clusters of cancerous cells (so-called tumor multicellular spheroids) represent an optimal biological test object because of their compact, spherical shapes and sizes of some 100 microns in diameter. The average scattering coefficient

#187031 - $15.00 USD Received 18 Mar 2013; revised 23 Apr 2013; accepted 23 Apr 2013; published 31 May 2013

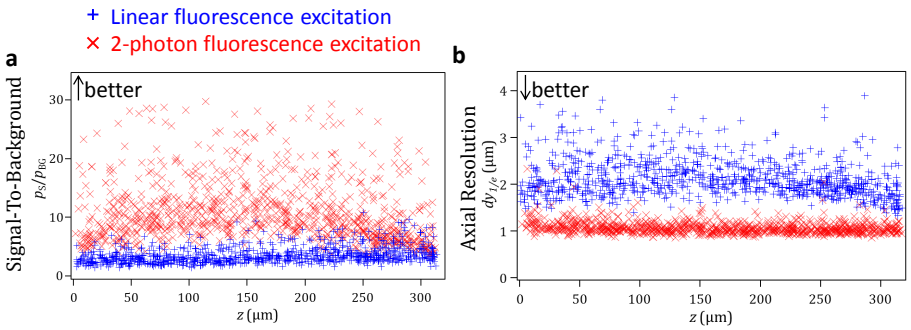

Fig. 7. **Signal-to-background analysis and axial widths of bead images.** (a) signal to background ratios $p_S/p_{\mathrm{BG}}(z)$ and (b) axial bead image widths $dy_{1/e}(z)$ are shown as a function of propagation distance z for 1200 beads (diameter $d = 0.75\mu$m). Results from the linear excitation are shown in blue (+) and for the two-photon excitation case in red (x).

of the spheroids is such that reasonable imaging from only one direction is possible, but on the other hand beam spreading is well visible and the self-reconstruction capability of Bessel beams are of great advantage. A deeper understanding of the mechanisms of spheroid growth will require investigating the main cellular components, such as actin filaments, that contribute to cell shape and motility. Here, we used tumor multicellular actin-labeled spheroids stained with Alexa-488 coupled to Phalloidin. We cultivated wild-type mouse colon carcinoma CT26 cells (American Tissue Culture Collection, ATCC CRL-2638). The spheroids were prepared by encapsulating and growing cells in spherical nutrient-permeable hydrogel shells up to a spheroid size of about 250μm in diameter. The cell-containing capsules were formed by a home-made co-extrusion device. The hydrogel is made of sodium alginate (FMC, Protanal LF200S) which is a biocompatible polysaccharide. Spheroids were then embedded in agarose gel cylinders and then illuminated with two different scanning Bessel beams at wavelengths of $\lambda_{1\mathrm{p}} = 488$nm and $\lambda_{2\mathrm{p}} = 920$nm.

Figure 8 shows images $p(x, y_0, z)$ of the same layer of a tumor multicellular spheroid illuminated with three different illumination beams. The images were acquired in a plane $s_y = 120\mu$m inside the spheroid as indicated by the inset of Fig. 8(a). Illumination with Bessel beams provides more signal in the back part of the spheroids. This finding is confirmed quantitatively by the integrated image intensity line scans $p(z) = \sum_i p(x_i, y_0, z)dx$ shown in Fig. 8(d). The penetration depths of the Bessel beams of $d_{\mathrm{Bessel,1p}} \approx 338\mu$m and $d_{\mathrm{Bessel,2p}} \approx 562\mu$m (exponential fits $p \propto \exp\{-z/d\}$ in Fig. 8(d)) are enhanced by a factor of 2.2 and 3.7 relative to the penetration depth $d_{\mathrm{Gauss,1p}} \approx 152\mu$m of the Gaussian beam. The increase in penetration depth for Bessel beams by a factor of 1.7 is close to the theoretical prediction for predominantly Mie-Scattering samples made in the previous section (Eq. (12)).

8. Increased image contrast by confocal line detection

In addition, the contrast is best for the two-photon Bessel beam, i.e. the details provided by single cells in the back part of the spheroid, are best visible with two-photon excitation. A more detailed contrast analysis is possible by investigating the ratio of high-frequency and low-frequency image information. Corresponding to the method of Truong [14], the images $p(x,z)$ are Fourier transformed to $\tilde{p}(k_x, k_z) = FT[p(x,z)]$ and separated into images with high spatial frequencies (HSF, where $k_r = \sqrt{k_x^2 + k_y^2} \geq k_F$) and low spatial frequencies (LSF, where $k_r = \sqrt{k_x^2 + k_y^2} \leq k_F$) defined by the corner frequency $k_F = 1/2\mu$m. The ratio of the average

#187031 - $15.00 USD Received 18 Mar 2013; revised 23 Apr 2013; accepted 23 Apr 2013; published 31 May 2013

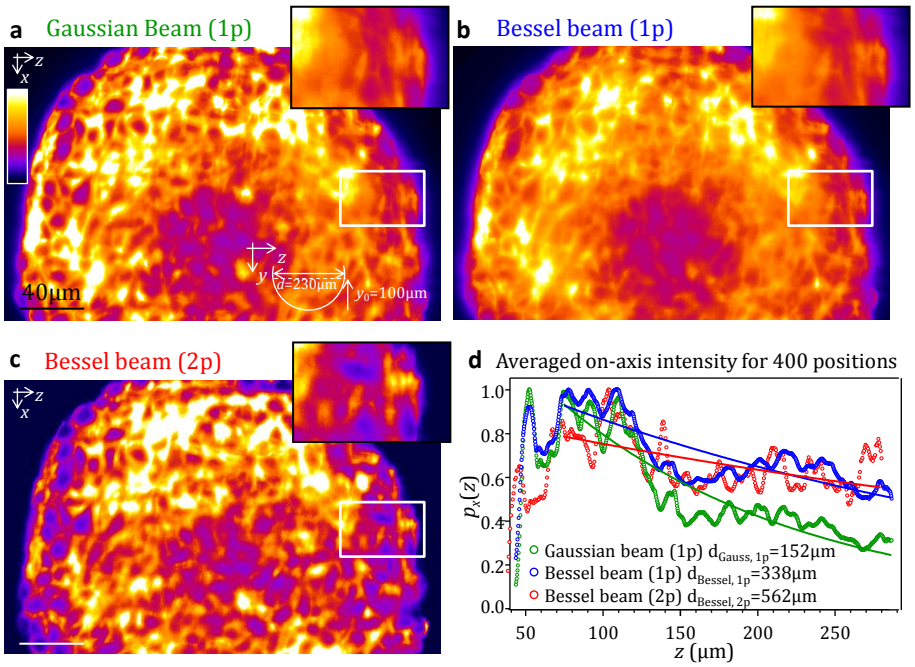

Fig. 8. **Images of a tumor multicellular spheroid for scanned illumination beams.** a-c) show slices $p(x,y_0,z)$ from the same tumor multicellular spheroid with a diameter of 230 μm. The insets show magnified parts at the back side of the spheroid that are marked by white boxes. The images were acquired $y_0 = 100\mu$m inside the spheroid. All beams which are a) 1p- Gaussian beam, b) 1p- Bessel beam and c) 2p- Bessel beam have the same depth of field and propagate from left or right. d) shows the intensity decay $p(z)$ along the propagation z-direction for single illumination beams, acquired by multiplication of the images of the static beam at 400 positions with a Gaussian mask ($1/e$-width of 750nm) and integration along x.

high-pass and low-pass filtered intensities $\left|\tilde{p}(k_x,k_y)\right|$ provides a quality parameter for image contrast Q_{con} , which is defined by

$$Q_{\mathrm{con}} = \frac{\mathrm{HSF}}{\mathrm{LSF}} = \frac{\int_{k_r \geq k_F} |\tilde{p}(k_x,k_z)|\,\mathrm{d}k_x\mathrm{d}k_z}{\iint_{k_r<k_F} |\tilde{p}(k_x,k_z)|\,\mathrm{d}k_x\mathrm{d}k_z} \tag{15}$$

This expression represents an alternative signal-to-background ratio and effectively describes the usable in-focus intensity signals HSF relative to the image out-of-focus intensity LSF. We investigated the decrease in contrast $Q_{\mathrm{con}}(y_i)$ for different image planes $p(x,y_i,z)$ along the detection direction y, all generated with Bessel beams and two-photon fluorescence excitation. Furthermore we compared the conventional widefield detection mode, where a Bessel beam is scanned laterally during the illumination time of the CCD camera (scan-mode), with a confocal-line detection mode (CL-mode) as described in [6]. The selected image planes $p(x,y_i,z)$ at two different heights ($y_i = 120\mu$m and $y_i = 50\mu$m) are shown in Fig. 9(a-d) for both the scan mode (left) and the CL-mode (right). The CL-mode further increases the signal-to-background ratio $Q_{\mathrm{con}}(y_i)$ as displayed in Fig. 9(e). It also demonstrates that the contrast $Q_{\mathrm{con}}(y_i)$ depends only weakly on the height y_i of the image plane inside the spheroid. Figure 9(e) further exhibits that the contrast $Q_{\mathrm{con}}(y_i)$ is significantly better in images illuminated by two-photon Bessel beams relative to single-photon Bessel beams.

#187031 - $15.00 USD Received 18 Mar 2013; revised 23 Apr 2013; accepted 23 Apr 2013; published 31 May 2013

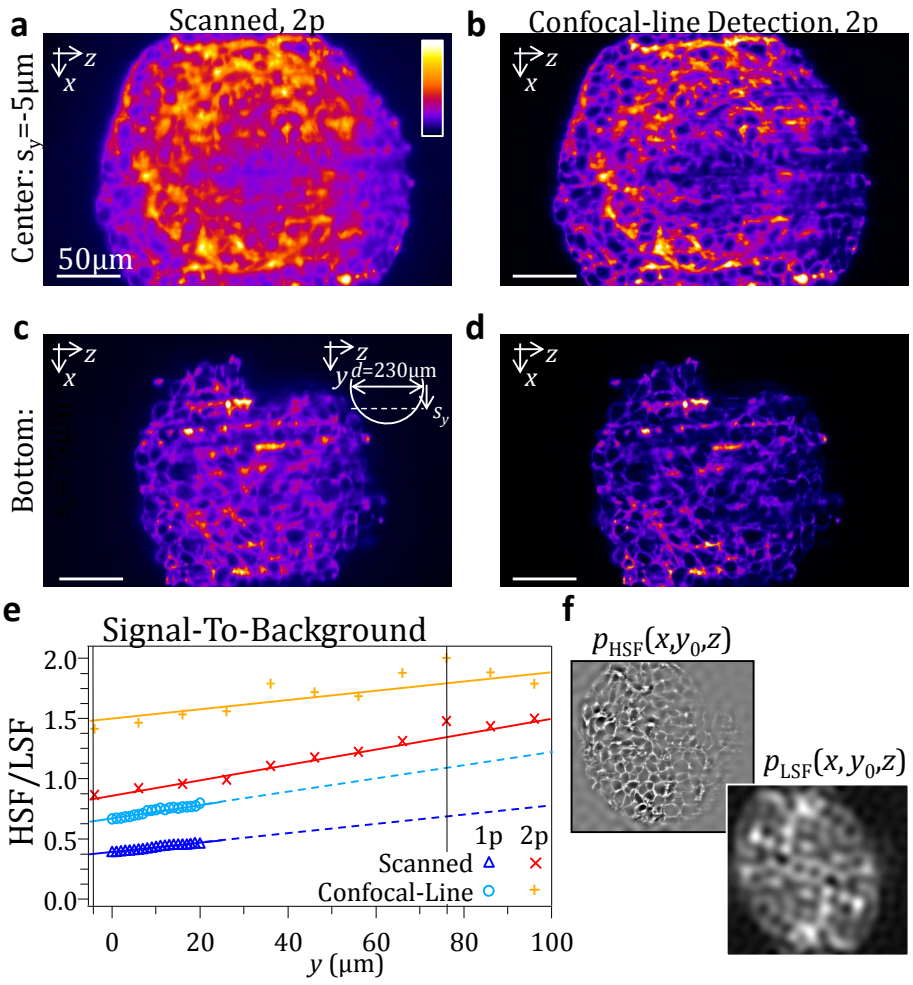

Fig. 9. **2p-Images of a tumor multicellular spheroid with and without confocal line detection.** Image slices $p(x,y_0,z)$ from the same spheroid illuminated by a Bessel beam and two-photon fluorescence excitation. Image planes were required at $y_0 = 120\mu$m (top row) and $y_0 = 40\mu$m (bottom row) inside the spheroid. Fluorescence images were acquired by a scanned illumination beam (a,c) and by confocal line-detection (b,d). e) The signal-to-background $Q_{\mathrm{con}}(y_i) = \mathrm{HSF}(y_i)/\mathrm{LSF}(y_i)$ generated from four different illumination and detection schemes for various image planes in detection direction y_i. Examples for the high- and low-pass filtered images, $p_{\mathrm{HSF}}(x,y_0,z)$ and $p_{\mathrm{LSF}}(x,y_0,z)$ that used to generate the contrast parameter $Q_{\mathrm{con}} = \mathrm{HSF}/\mathrm{LSF}$ are shown in (f).

9. Summary and conclusion

We have successfully demonstrated how the image quality in light-sheet based microscopy can be significantly increased by using scanned Bessel beams and two-photon fluorescence excitation (TPE). In several hundred microns large clusters of spheres and of cells we could validate the self-reconstruction ability and increased penetration depth of Bessel beams for both visible and NIR-wavelengths. While the ring system of the Bessel beam is maintained on the excitation side, fluorescence from the ring system is strongly suppressed due to the quadratic dependence of the illumination intensity.

#187031 - $15.00 USD Received 18 Mar 2013; revised 23 Apr 2013; accepted 23 Apr 2013; published 31 May 2013

Although TPE by Bessel beams in a light-sheet microscope was used to generate high-quality images of small samples with sizes $< 50\mu$m [4], and in large but modestly scattering C.elegans samples [5], the benefits in large and strongly scattering media were not exploited so far. Moreover, Truong et al. [14] achieved best results for imaging large drosophila embryos, when using a scanned Gaussian beam and two-photon excitation, but did not investigate Bessel beams. Olarte et. al. [5] presented an interesting technical approach to a setup that allows linear and two-photon excitation (TPE) by both Gaussian and Bessel beams, but they did not investigate the performance differences for beams with equal depth of field. The depth of field of the illumination beam is the determining parameter for efficient use in a light-sheet microscope.

In particular, we estimated and showed that the penetration depth and axial fluorescence decay of the Bessel beam at $\lambda = 800$nm is superior to that of a Bessel beam at 488nm. Whereas linear excitation by Bessel beams shows a 2-fold increased penetration depth, TPE by Bessel beams reveals a 3-4 fold increased penetration depth relative to a comparable Gaussian beam in tumor multicellular spheroids. TPE by Bessel beams increases the signal-to-background ratio by 30% - 90% relative to the linear case for equal depths of field. These proof-of-principle results represent rough estimates of the performance of linear and two-photon Bessel beams and will vary for different cell clusters or specimen.

In a cluster of $d = 0.75\mu$m latex spheres the signal-to-background ratio was even increased by a factor of 5-10 and the axial resolution (detection direction) was nearly doubled relative in the TPE relative to the linear case for Bessel beams, again with equal depth of field. Most experimental results were confirmed by results from computer simulations using the beam propagation method (BPM), which provide a better understanding of the differences between the hypothetical ideal image and the real image containing artifacts due to scattering and interference.

So far no experiments have been performed to explicitly compare the fluorophore bleaching in biological specimen when using linear or two-photon excitation by Bessel beams. By normalizing on the same intensity signal, it has been shown that about 6 times more energy is deposited in to the sample by Bessel beam illumination relative to Gaussian beam illumination [6]. However, Bessel beams provide a higher axial resolution and less background when using confocal-line detection. From a theoretical view-point, excitation and destruction of fluorophores in the Bessel beam's ring system is less probable due to the reduced intensity in the ring system. Due to the reduced photon energy, it is even more unlikely for two-photon excitation with NIR-light. However, over-all bleaching strongly depends on the used labeling, laser-wavelengths and pulses as well as illumination patterns and needs to be investigated separately for each case. Imaging of multi-cellular spheroids, though, seems to benefit strongly from light-sheet microscopy using TPE Bessel beams and may open new doors for the investigation of their multi-cellular dynamics and mechanics.

10. Append: Depth of field of Bessel beams for single- and two-photon excitation

Here we briefly discuss the requirements to adjust a 1p- and 2p- Bessel beams such that they have the same depth of field and the same width of the central main lobe. Adjustment is possible by tuning the focusing angle α by the NA $= n\sin(\alpha)$ of the illumination lens and by the parameter ε for thickness of the ring spectrum in the BFP of the illumination lens. For homogeneous (annular or circular) illumination of the back-focal plane, the axial profile at the object for linear fluorescence excitation is

$$\begin{aligned} F_{1p}(z) &= c_F \cdot \sigma_{1p} \cdot h_{ill,1}(z) \\ &= c_F \cdot \sigma_{1p} \cdot I_{0,1} \cdot \mathrm{sinc}(2\pi \cdot z/\Delta z_{1p})^2. \end{aligned} \tag{16}$$

#187031 - $15.00 USD Received 18 Mar 2013; revised 23 Apr 2013; accepted 23 Apr 2013; published 31 May 2013

The corresponding two-photon fluorescence excitation profile is

$$\begin{aligned} F_{2\mathrm{p}}(z) &= c_F \cdot \sigma_{2\mathrm{p}} \cdot h_{\mathrm{ill},2}(z)^2 \\ &= c_F \cdot \sigma_{2\mathrm{p}} \cdot I_{0,2}^2 \cdot \mathrm{sinc}(2\pi \cdot z/\Delta z_{2\mathrm{p}})^4. \end{aligned} \tag{17}$$

The full-width at half of the maximum intensity I_0 (FWHM) in axial direction can be found by setting: $F_{1\mathrm{p}}(\Delta z_{1\mathrm{p}}) = F_{1\mathrm{p}}(0)/2$ and $F_{2\mathrm{p}}(\Delta z_{2\mathrm{p}}) = F_{2\mathrm{p}}(0)/2$. It follows that

$$\Delta z_{1\mathrm{p}} = \frac{0.88 \cdot \lambda_1}{\left(\sqrt{n^2 - \varepsilon_1 \mathrm{NA}_1^2} - \sqrt{n^2 - \mathrm{NA}_1^2}\right)} \approx \frac{1.76\, n\, \lambda_1}{\mathrm{NA}_1^2 (1 - \varepsilon_1)} \tag{18}$$

and

$$\Delta z_{2\mathrm{p}} = \frac{0.64 \cdot \lambda_2}{\left(\sqrt{n^2 - \varepsilon_2 \mathrm{NA}_2^2} - \sqrt{n^2 - \mathrm{NA}_2^2}\right)} \approx \frac{1.28\, n\, \lambda_2}{\mathrm{NA}_2^2 (1 - \varepsilon_2)}. \tag{19}$$

For the approximation the expansion for small values of ε can be used, since $\varepsilon < 1$ by definition. From eqns (18) and (19) above and taking into account that different wavelengths are used to excite the same dye by linear and two-photon processes, the ratio of the depth of field for linear and nonlinear fluorescence excitation is $\Delta z_{1\mathrm{p}}/\Delta z_{2\mathrm{p}} = 1.39 \cdot \lambda_2/\lambda_1$. To obtain 1p- and 2p-fluorescence excitation profiles $F(z)$ with equal depth of field the NA and/or the ring parameter ε can be adapted. An equal depth of field $\Delta z_{1\mathrm{p}} = \Delta z_{2\mathrm{p}}$ requires adaptation of the ring thickness parameter according to

$$\varepsilon_2 = 1 + 0.73 \cdot (\varepsilon_1 - 1) \cdot \frac{\lambda_2}{\lambda_1} \frac{\mathrm{NA}_1^2}{\mathrm{NA}_2^2} \approx -0.45 + 1.45\varepsilon_1 \tag{20}$$

The latter approximation is valid for a constant numerical aperture $\mathrm{NA}_1 = \mathrm{NA}_2$ and when $\lambda_2 = 2\lambda_1$.

Acknowledgments

We thank Dr. Roland Nitschke for help with the Coherent Chameleon laser and Cristian Gohn-Kreuz for carefully reading the manuscript and helpful discussions. This work was financed by the Baden-Württemberg Stiftung.

#187031 - $15.00 USD Received 18 Mar 2013; revised 23 Apr 2013; accepted 23 Apr 2013; published 31 May 2013